THE JOURNAL OF PHYSICAL CHEMISTRY A
A JOURNAL OF THE AMERICAN CHEMICAL SOCIETY

pubs.acs.org/JPCA Article

Excited-State Bond Contraction and Charge Migration in a Platinum Dimer Complex Characterized by X-ray and Optical Transient Absorption Spectroscopy

Nicholas P. Weingartz, Michael W. Mara, Subhangi Roy, Jiyun Hong, Arnab Chakraborty, Samantha E. Brown-Xu, Brian T. Phelan, Felix N. Castellano,* and Lin X. Chen*

Cite This: https://doi.org/10.1021/acs.jpca.1c07201 Read Online

ACCESS | Metrics & More | Article Recommendations | Supporting Information

ABSTRACT: Interactions between metal centers in dimeric transition metal complexes (TMCs) play important roles in their excited-state energetics and pathways and, thus, affect their photophysical properties relevant to their applications, for example, photoluminescent materials and photocatalysis. Here, we report electronic and nuclear structural dynamics studies of two photoexcited pyrazolate-bridged $[Pt(ppy)(\mu\text{-}R_2pz)]_2$-type Pt(II) dimers (ppy = 2-phenylpyridine, μ-R_2pz = 3,5-substituted pyrazolate): $[Pt(ppy)(\mu\text{-}H_2pz)]_2$ (**1**) and $[Pt(NDI\text{-}ppy)(\mu\text{-}Ph_2pz)]_2$ (**2**, NDI = 1,4,5,8-naphthalenediimide), both of which have distinct ground-state Pt−Pt distances. X-ray transient absorption (XTA) spectroscopy at the Pt L_{III}-edge revealed a new d-orbital vacancy due to the one-electron oxidation of the Pt centers in **1** and **2**. However, while a transient Pt−Pt contraction was observed in **2**, such an effect was completely absent in **1**, demonstrating how the excited states of these complexes are determined by the overlap of the Pt (d_{z^2}) orbitals, which is tuned by the steric bulk of the pyrazolate R-groups in the 3- and 5-positions. In tandem with analysis of the Pt−Pt distance structural parameter, we observed photoinduced electron transfer in **2** featuring a covalently linked NDI acceptor on the ppy ligand. The formation and subsequent decay of the NDI radical anion absorption signals were detected upon photoexcitation using optical transient absorption spectroscopy. The NDI radical anion decayed on the same time scale, hundreds of picoseconds, as that of the d-orbital vacancy signal of the oxidized Pt−Pt core observed in the XTA measurements. The data indicated an ultrafast formation of the charge-separated state and subsequent charge recombination to the original Pt(II−II) species.

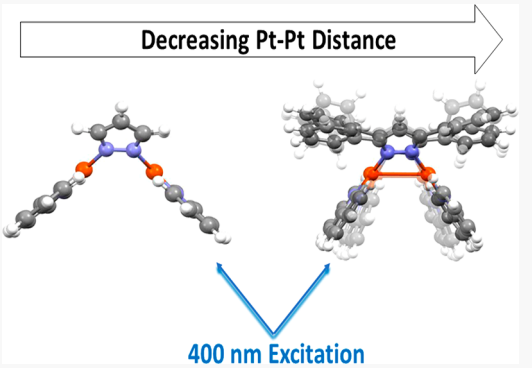

INTRODUCTION

Bimetallic transition metal complexes (TMCs) bridged by heterocyclic ligands represent a class of compounds that have shown promise as photoluminescent sensors,[1,2] photocatalysts,[3,4] and light emitters, particularly in organic light-emitting diodes (OLEDs).[5,6] Among the most interesting bimetallic TMCs for OLED applications are those containing Pt(II) centers due to their long-lived triplet excited states and high photoluminescence emission quantum yields.[6,7] Pt(II) dimer complexes and their various mononuclear aggregates have emerged as candidates for new photoluminescent materials, with a key structural factor being the Pt−Pt interaction.[8−12] Along with favorable excited-state lifetimes and luminescent quantum efficiencies, Pt(II) dimers of the form $[Pt(ppy)(\mu\text{-}R_2pz)]_2$ [ppy = 2-phenylpyridine, μ-R_2pz = 3,5-substituted pyrazolate], with the so-called "butterfly-like" geometry,[13−15] exhibit tunability of their photophysical properties, in particular absorption and emission spectra, by changing the steric bulk of the R-group, thus altering the Pt−Pt distance and hence the HOMO−LUMO gap.

Square-planar monomeric Pt(II) complexes exhibit HOMO−LUMO transitions comprising ligand-centered (LC) and/or metal-to-ligand charge-transfer (MLCT) transitions.[16] In a Pt(II) dimer or aggregate, a new electronic transition emerges from the overlapping out-of-plane Pt(II) d_{z^2} orbitals to higher unoccupied orbitals as the Pt−Pt distance shortens sufficiently, as observed in the $[Pt_2(H_2P_2O_5)_4]^{4-}$ (Ptpop) complexes.[17−19] The interacting $5d_{z^2}$ orbitals from two adjacent Pt(II) atoms form the σ bonding and σ^* antibonding orbitals, with the latter dominating the HOMO. The new electronic transition, denoted as a metal−metal-to-ligand charge-transfer (MMLCT) transition, consists of excitation from the metal−metal centered d_{σ^*}, or HOMO,

Received: August 13, 2021
Revised: September 16, 2021

orbital to the ppy ligand π^*, or LUMO, orbital, resulting in a transient Pt−Pt bond formation between two Pt atoms with a nominal bond order of 0.5. The framework of $[Pt(ppy)(\mu\text{-}R_2pz)]_2$-type Pt dimers allows tunability of the Pt−Pt distance by varying the size of the R hinge group, thus controlling the level of interaction between the two Pt centers.[15] Furthermore, transient localization of charge on the ppy ligand[20] through the MMLCT transition offers an opportunity to decorate these ligands with electron acceptors in order to initiate electron transfer away from the Pt(II) dimer framework, similar to a prior study of a monomeric Pt(II) complex by Sazanovich et al.[21]

In previous studies, optical spectroscopy[14,15,22] and quantum density functional theory (DFT) calculations[23−25] were used to characterize the excited-state dynamics as a function of Pt−Pt distance following MMLCT excitation in a series of these Pt(II) dimer complexes. X-ray transient absorption (XTA) spectroscopy and wide-angle X-ray scattering (WAXS) in solution revealed a Pt−Pt contraction of 0.3−0.5 Å following MMLCT excitation for one of the pyrazolate Pt(II) dimer complexes.[26,27] Other studies using optical transient absorption (OTA) spectroscopy and transient absorption anisotropy spectroscopy have indirectly probed the structural dynamics by identifying vibrational coherence in a Pt−Pt stretching mode present in various MMLCT-presenting Pt(II) "butterfly-like" dimers, which manifests as an oscillatory modulation in the OTA signal.[28−31]

Here, we present a study of two $[Pt(ppy)(\mu\text{-}R_2pz)]_2$-type complexes (Figure 1) to establish a structural basis in the

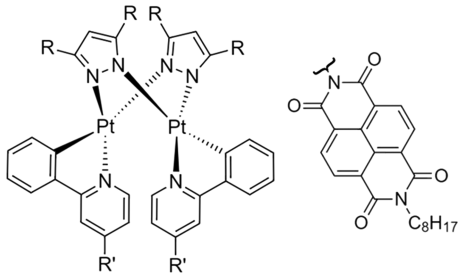

Figure 1. Structure of systems **1** and **2** (left) and the structure of the NDI acceptor group (right).

excited state between Pt(II) dimers featuring monomer-like LC/MLCT transitions due to sufficiently separated Pt(II) centers and those with MMLCT transitions due to strongly interacting metal centers. It has been asserted that $[Pt(ppy)(\mu\text{-}H_2pz)]_2$(**1**) would exhibit no significant structural reorganization upon photoexcitation due to the absence of the Pt−Pt d_{z^2} overlap, which should preclude transient bond formation;[13,15] however, structure-sensitive measurements on **1** have yet to be performed to date. Conversely, $[Pt(ppy)(\mu\text{-}Ph_2pz)]_2$ would exhibit structural reorganization as the Pt(II) centers are sufficiently close to facilitate interaction between the Pt $5d_{z^2}$ orbitals and, thus, transient bond formation upon photoexcitation. X-ray diffraction revealed ground-state Pt−Pt distances of 3.27 Å for **1** and 2.98 Å for $[Pt(ppy)(\mu\text{-}Ph_2pz)]_2$,[23] corresponding well with those obtained from DFT calculations, 3.49 and 3.16 Å,[13] respectively. Additionally, we investigated the feasibility of photoinduced electron transfer (PET) away from the Pt−Pt core by covalently linking the electron acceptor 1,4,5,8-naphthalenediimide (NDI) to each of the ppy ligands in the complex $[Pt(NDI\text{-}ppy)(\mu\text{-}Ph_2Pz)]_2$ (**2**).

To capture the transient structures of these complexes, XTA spectroscopy was employed in both the X-ray absorption near-edge structure (XANES) and extended X-ray absorption fine structure (EXAFS) regions to identify electronic and nuclear structural changes at the X-ray absorbing Pt centers of **1** and **2**. For **2** in particular, the combined OTA and XTA spectroscopic results reveal the kinetics of electronic structural change in the presence of the electron acceptor NDI. The excited-state and charge-separated (CS) state structural characterizations in this study are critical in unraveling the complex excited-state dynamics of "butterfly-like" Pt(II) dimers by providing a concrete analysis of structural changes upon photoexcitation for both LC/MLCT and MMLCT-presenting complexes as well as providing a foundation for extracting charge from the Pt(II−II) core.

METHODS

Materials. The Pt(II) dimers **1**, $[Pt(ppy)(\mu\text{-}H_2pz)]_2$, and **2**, $[Pt(NDI\text{-}ppy)(\mu\text{-}Ph_2pz)]_2$, were prepared by adapting established literature procedures. The synthetic protocol for **1** was originally described by Rachford et al.,[15] and the synthetic procedure for **2** is provided in the Supporting Information (Figures S1−S6). Inhibitor-free anhydrous tetrahydrofuran (>99.9%) solvent was purchased from Sigma-Aldrich and used without further purification.

Static Absorption Measurements. Steady-state UV−vis absorption spectra were acquired using a Cary 60 spectrophotometer.

Optical Transient Absorption Spectroscopy. Ultrafast OTA experiments were conducted as described in previous publications[13,32] using a commercial Ti:sapphire oscillator with a regenerative amplifier (Spectra-Physics). The Spitfire Pro XP regenerative amplifier, seeded with a Mai-Tai oscillator (Spectra-Physics), was operated at 1 kHz and output a 2.9 mJ beam with a pulse duration of 100 fs at the full-width at half-maximum and centered at 830 nm. The output beam was split and then frequency doubled using a 2 mm-thick type I lithium triborate crystal ($\theta = 90°$, $\varphi = 28°$) to yield the 415 nm pump. The other portion was focused into a sapphire window to generate the continuum probe (450−800 nm).

The OTA signal was detected using a Helios pump−probe spectrometer and software (Ultrafast System LLC), and pump on/off spectra were obtained using a mechanical chopper operating at 500 Hz. The 415 nm pump pulse had an energy of 0.6 μJ at the sample and overlapped with the probe beam at an angle of 10°. Samples were dissolved in degassed THF and loaded into a 2.0 mm quartz cuvette. Sample concentrations were adjusted so that the absorbance at λ_{max} of the MMLCT transition was ∼0.5. A magnetic stirrer and bar were used during data collection to prevent sample degradation under the beam.

Chirp correction and background subtraction were done in the commercial software Surface Xplorer (Ultrafast Systems LLC). Chirp correction parameters were extracted from the nonresonant solvent response at t_0. Kinetics traces at selected probe wavelengths were analyzed using a laboratory-written Python program and fit to a sum of exponential functions convolved with a Gaussian instrument response function (IRF); the IRF duration is given as the full-width at half-maximum values in the discussion below. Decay-associated spectra (DAS) were also generated from the full data sets in

https://doi.org/10.1021/acs.jpca.1c07201
J. Phys. Chem. A XXXX, XXX, XXX−XXX

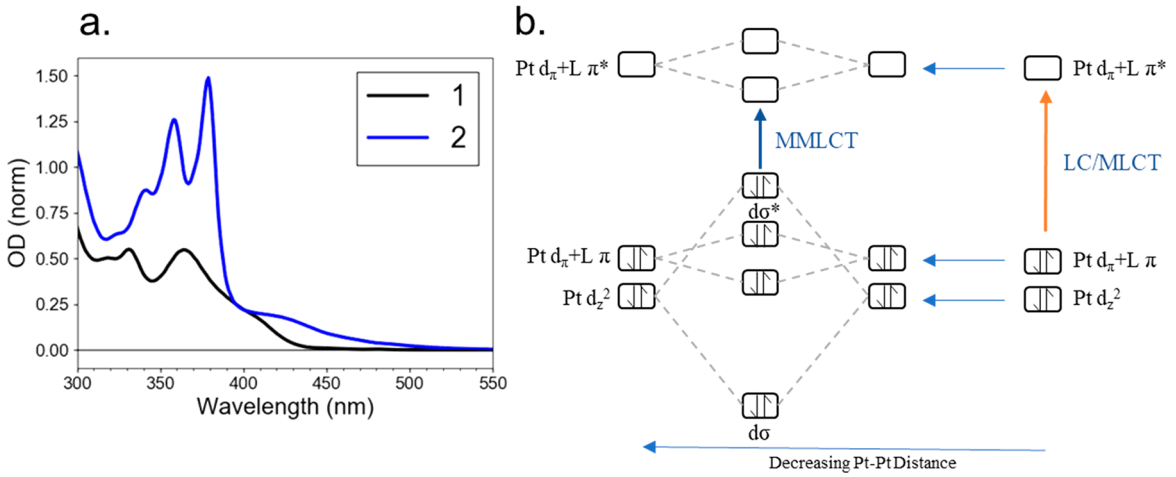

Figure 2. (a) Steady-state absorption normalized to show LC/MLCT and MMLCT features (b) corresponding MO transitions of **1** and **2**.

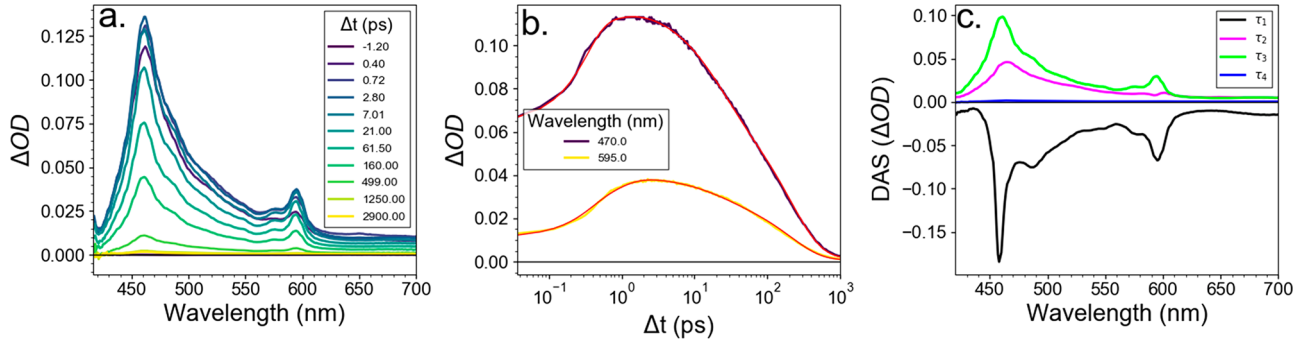

Figure 3. Optical transient absorption of **2** (a) at various time delays (λ_{ex} = 415 nm), (b) kinetic traces at λ = 470 nm and λ = 595 nm, and (c) decay-associated spectra of τ_{1-4}.

this custom software using the time-dependent amplitudes for each exponential component extracted with the kinetic fitting.

X-ray Transient Absorption Spectroscopy. XTA measurements were carried out at beamline 11-ID-D of the Advanced Photon Source at Argonne National Laboratory as described in previous publications.[33,34] The monochromator was a Si(111) double crystal with a resolution of $\Delta E/E = 10^{-4}$. The sample was excited by 400 nm laser pulses at 10 kHz repetition rate from the second-harmonic output of a Ti:sapphire laser system (Coherent Lasers, Micra-5 Oscillator, Legend Elite Duo Regenerative Amplifier). The laser beam was focused to a 0.75 mm × 0.6 mm spot size, and the X-ray spot size was 0.2 mm × 0.5 mm at the sample. The laser pulse energy at the sample for **1** was set to 24.3 μJ, and the laser power at the sample on **2** was set at 43 μJ to ensure linear signal vs pulse energy correlation and to avoid sample degradation. The 24-bunch mode of the APS was used with the total current of 100 mA and inter-X-pulse separation of 153 ns. The time delay between the laser pump pulse and X-ray probe pulse was set to nominally 100 ps, which was sufficient for capturing the triplet MMLCT state and CS state in **1** and **2**. XTA spectra were collected in fluorescence mode using two avalanche photodiodes, one on each side of the sample jet, at 90° angles to the incident X-ray beam. The Pt dimers were dissolved in anhydrous THF, and, due to differing levels of solubility, **1** was prepared at 1 mM and **2** was prepared at 0.2 mM. The samples were purged with nitrogen gas throughout of the measurements and flowed through a liquid jet with a stream thickness of ~0.5 mm. Elastic scattering was attenuated using soller slits packed with three absorption lengths of Zn. A Pt foil was placed behind the sample jet and before an ion chamber to measure the X-ray transmission concurrently for energy calibration. XTA data analysis was performed using the Athena and Artemis program packages[35,36] with spline fitting performed in the program PySpline.[37] Detailed fitting information can be found in the Supporting Information

RESULTS AND DISCUSSION

Static UV−vis Absorption Measurements. UV−vis absorption spectra of **1** and **2** normalized to the lowest energy feature are shown in Figure 2a. The spectra of both **1** and **2** have shoulders that extend past 400 nm to longer wavelengths, with the shoulder of **2** extending further toward 500 nm than that of **1**. The feature in **1** from ~350 nm to ~430 nm, including the shoulder, corresponds to the LC/MLCT excitation.[13] The spectral features in **2** from ~320 nm to ~395 nm are characteristic of absorption from the NDI moiety[38] (Figure S7). The broad shoulder from ~400 nm to ~480 nm indicates the introduction of an MMLCT transition in **2** at a lower energy than the LC/MLCT transition in **1**. This MMLCT band is also present in an analogous Pt dimer (R = Ph) without NDI electron acceptors[13] (Figure S7). A molecular orbital (MO) scheme showing the change from LC/MLCT excitation to MMCLT excitation upon shortening of the Pt−Pt distance is presented in Figure 2b.

Optical Transient Absorption Spectroscopy. The OTA spectra of **2** are shown in Figure 3a. The OTA spectra exhibit broad absorption throughout the visible range, with sharp

https://doi.org/10.1021/acs.jpca.1c07201
J. Phys. Chem. A XXXX, XXX, XXX−XXX

peaks at 460 and 595 nm. Kinetics traces at the two prominent OTA peaks were fit simultaneously with a multiexponential model (Figure 3b,c), and the results of this global fitting were used to extract the decay-associated spectra (DAS) shown in Figure 3c. Both peaks rise with a time constant of τ_1 = 0.46 ps and then decay with time constants of τ_2 = 20.1 ps and τ_3 = 206 ps (Table 1). There is a long-lived component, τ_4, with about 1% of the initial absorption amplitude that persists on time scales past the range of the experimental time window (Figures 3c and S9).

Table 1. Lifetimes Extracted from Transient Optical and X-ray Spectra of 1 and 2

	complex 1			complex 2			
method	τ_1 (ps)[a]	τ_2 (ps)[b]	τ_3[c]	τ_1 (ps)[a]	τ_2 (ps)[b]	τ_3 (ps)[c]	τ_4[d]
OTA	0.38	13.8	0.75 μs	0.46	20.1	206	$\gg$ 3 ns
XTA	–	–	$\gg$1 ns	–	–	520	–

[a]ISC in **1** and formation of CS state in **2** with the XTA results limited by the instrument response time of ~100 ps. [b]Structural reorganization in **1** and structural reorganization, vibrational cooling, and solvation in **2**. [c]Decay of ^{3}LC/MLCT in **1** and CS state decay in **2**. [d]Decay of long-lived CS in **2**.

The locations of the prominent excited-state absorption peaks at 460 and 595 nm agree with literature values for the NDI radical anion ($NDI^{\bullet-}$).[39] This result shows that upon excitation, the electron from the platinum σ^* orbital is transferred to an orbital centered on the NDI acceptor groups attached to the ppy ligand. The $NDI^{\bullet-}$ features appear within the 0.56 ps instrument response, indicating a subpicosecond localization of charge on the NDI groups. The DAS of τ_1, shown in Figure 3c, consists of negative amplitude at the $NDI^{\bullet-}$ peaks, which corresponds to formation of those features, and is consistent with subpicosecond electron localization on NDI. In these "butterfly-like" Pt dimer TMCs, ISC from the ^{1}MMLCT to ^{3}MMLCT occurs on the order of magnitude of hundreds of femtoseconds,[29] which may be the same time scale as electron transfer to the NDI in **2**. This suggests that there may be two competing excited-state trajectories upon excitation into the ^{1}MMLCT state of **2**, one that first proceeds to undergo ISC to a ^{3}MMLCT state before CS occurs and another that proceeds to the electron transfer state directly from the ^{1}MMLCT state.

The rise of the $NDI^{\bullet-}$ features is followed by a 20.1 ps lifetime corresponding to structural reorganization of the complex to its lowest energy conformation as well as vibrational cooling. This is evidenced by the DAS component for τ_2 (Figure 3c), which has red-shifted $NDI^{\bullet-}$ features when compared to the longer-lived τ_3 component and a first-derivative-like feature at 600 nm. These features in the τ_2 DAS indicate relaxation in orbital energy over this period. The DAS component for τ_2 also has an amplitude equal to one-third of the total amplitude of absorption, indicating significant charge recombination within 20.1 ps. Upon structural reorganization, possibly rotation about the bond between the NDI and ppy to a less planar conformation, orbital overlap between the $NDI^{\bullet-}$ and the oxidized Pt dimer moiety decreases, leading to less favorable charge recombination. The remaining CS state population then decays back to the ground state with a lifetime of 206 ps. Decay back to the ground state is substantially faster in **2** than in **1** (Figure S8), proceeding in under 1 ns in **2** and nearly 1 μs in **1**. Charge recombination at

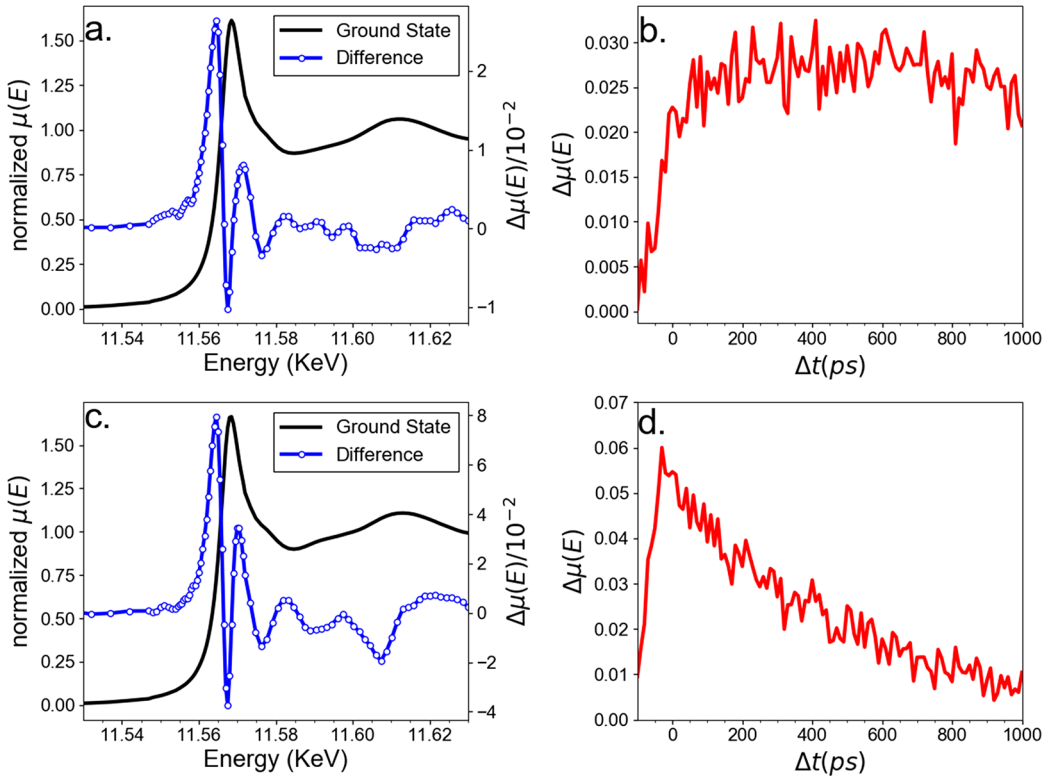

Figure 4. Ground-state XANES with excited-state difference spectra (excited minus ground) of **1** (a) and **2** (c) and XTA kinetic traces at energy of 11.561 keV of **1** (b) and **2** (d).

https://doi.org/10.1021/acs.jpca.1c07201
J. Phys. Chem. A XXXX, XXX, XXX−XXX

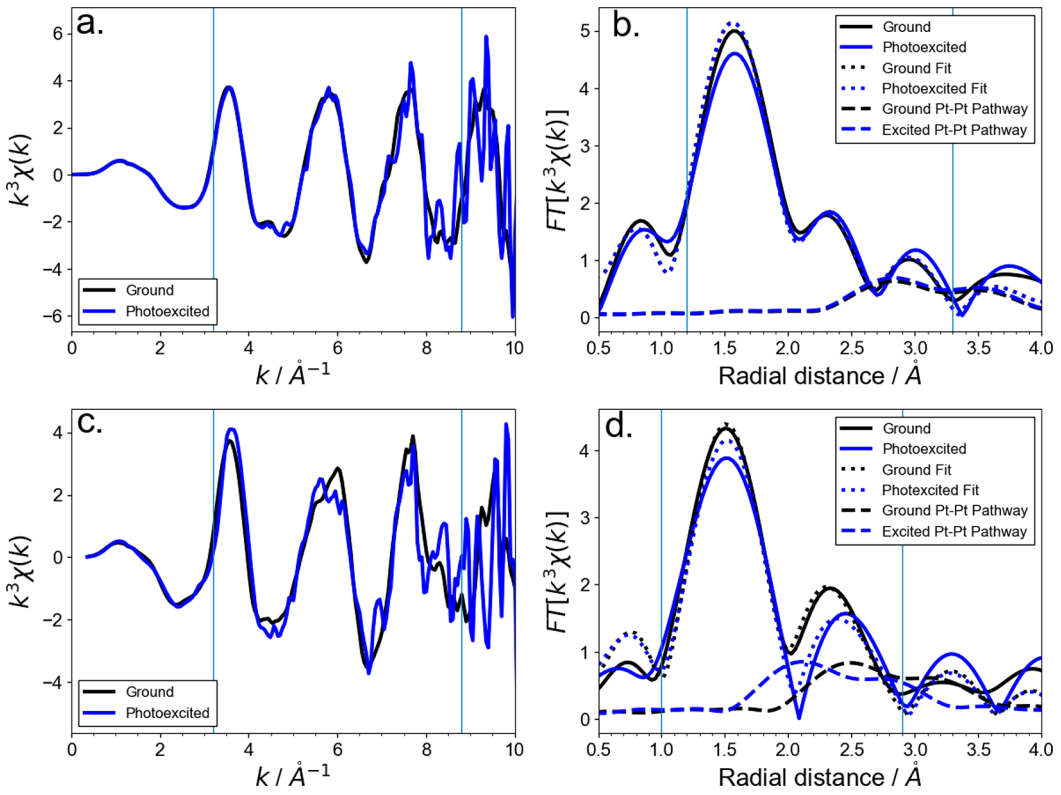

Figure 5. Ground and excited EXAFS spectra of **1** (a, b) and **2** (c, d) in *k*-space and *R*-space. *R*-space plots (b, d) include fits and Pt−Pt scattering pathways. Solid blue vertical lines represent FT range (a, c) and fitting range (b, d).

this time scale has previously been observed in TMCs attached to related rylene mono- and diimide acceptors.[40−42] The complete excited-state dynamics of **2** without NDI, [Ptppy)(μ-Ph_2pz)]$_2$, were previously reported by Brown-Xu et al.[13] and have been reproduced in Table S2.

The ultrafast OTA difference spectra of **1** are shown in Figure S8. The major peak at 445 nm rises well within the 0.42 ps instrument response and has a broad tail feature that extends out to 800 nm. The decreased positive absorption feature seen at wavelengths below 445 nm is due to the ground-state bleaching signal. As the system relaxes, the peak at 445 nm begins to sharpen with a time constant of τ_1 = 0.38 ps, while the tail feature decays. Subsequently, a shoulder arises at 490 nm as the sharp peak at 445 nm decays further with a time constant of τ_2 = 13.8 ps. No significant spectral changes follow as the system decays back to the ground with a time constant of τ_3 = 0.75 μs,[15] based on photoluminescence decay measurements from Rachford et al.[15] Mewes et al.[29] showed that intersystem crossing (ISC) occurs in hundreds of femtoseconds in the analogous [Pt(ppy)(μ-^{t}Bu$_2$pz)]$_2$ complex. Thus, we assign the 0.38 ps process to ISC in **1** from the ^{1}LC/MLCT to ^{3}LC/MLCT state, followed by vibrational cooling with a 13.8 ps time constant in the ^{3}LC/MLCT state. The long-lived ^{3}LC/MLCT state then decays back to the ground state with a lifetime of 0.75 μs. While the time constants from this analysis are in agreement with our previous report on this complex,[13] the excited-state assignments have been updated to reflect the rapid ISC observed in a related complex.[29]

X-ray Transient Absorption Measurements. Pt L$_{III}$-edge (11.564 keV) XTA spectra were collected for both complexes to ascertain changes in the local electronic environment upon excitation with 400 nm light (Figure 4a,c). The XANES difference spectra (photoexcited − ground state) of **1** and **2** both show a sharp positive feature at 11.561 keV, a negative feature at the white line energy of 11.565 keV and then another positive feature at 11.567 keV. The Pt L$_{III}$-edge transition originates from the excitation of 2p electrons into the unoccupied 5d manifold. Upon valence photoexcitation by 400 nm photons, the MLCT transition in **1** and MMLCT transition in **2** deplete a 5d electron. Consequently, the positive feature at 11.561 keV emerges as a new 2p to 5d transition into the vacated 5d orbital.

To determine the lifetime of the 5d vacancy induced by the valence excitation, the time evolution of the difference XANES signal at 11.561 keV was measured for **1** and **2**, respectively, as shown in Figure 4b,d. The signal for **1** persists well past the 1 ns experimental window, whereas the signal for **2** decays with a time constant of 520 ps. Kinetic parameters extracted from OTA and XTA results based on exponential decay functions are tabulated in Table 1. The XTA kinetics scan for **1** (Figure 4b) shows that the Pt centers remain oxidized well beyond 1 ns with residual signals still seen at over 600 ns delay (Figure S9), in agreement with photoluminescence intensity decay measurements.[15] The energy of the CS state in **2**, (Pt−Pt)$^+$-NDI$^-$, is lower than that of the ^{3}MMLCT state of **2** without NDI by at least the driving force for CS. Thus, the energy gap of the CS state in **2** with the ground state is smaller than the ^{3}MMLCT state of **2** without NDI. Consequently, the 2 μs lifetime of the ^{3}MMLCT state of **2** without NDI[15] is significantly shortened in the charge recombination process, which is consistent with numerous TMC-based electron donor−acceptor dyads.[40,41] Both the OTA and XTA show excited-state decay in **2** on a 100s of ps time scale, considerably faster than that of **1**.

https://doi.org/10.1021/acs.jpca.1c07201
J. Phys. Chem. A XXXX, XXX, XXX−XXX

The nuclear structures of the MLCT state for **1** and the CS state for **2** have been investigated by analyzing the EXAFS spectra for the ground and photoexcited states of **1** and **2** shown in Figure 5. The EXAFS spectra for the photoexcited species consist of a mixture of ground-state and excited-state populations weighted by an excitation fraction, α. The *k*-space difference spectra of **1** and **2** (Figure S11) qualitatively illustrate the greater scattering difference between the ground and photoexcited spectra seen in **2** as compared to **1**. This is best demonstrated at $k > 4$ Å^{-1} where the difference signal intensity in Figure S11 is greater in **2** than **1**, indicating a higher magnitude change in geometry around the Pt atoms.

The EXAFS spectra in *k* and *R* spaces show no significant structural differences around the Pt centers after excitation of **1**, but differences are clearly visible for **2**. The details of the fitting procedure are described in the Supporting Information, along with the structural parameters extracted from the fits for the nearest and next-nearest neighboring atoms around each Pt atom (Tables S3 and S4) and plots of the fits for each EXAFS spectrum (Figures S13–S16). The Pt–Pt scattering pathways for ground and photoexcited spectra of **1** and **2** have been plotted in Figure 5b,d to illustrate the extracted changes in this path upon excitation. Pt–Pt distances obtained through EXAFS fitting, DFT calculations,[13] and crystal structures[23] are shown in Table 2. In the ground state, the Pt–Pt distance in **1** was fit at 3.34 Å and remained constant upon excitation. **2** exhibits a contraction of ~0.43 Å from 3.03 to 2.60 Å. These results agree with previous DFT predictions[13] of a negligible bond elongation between S_0 and T_1 states in **1** and a contraction of 0.43 Å between S_0 and T_1 states in NDI-free **2**.

Table 2. Pt–Pt Distances Determined through EXAFS Analysis Compared to Literature DFT[13] and Crystal Structure[23] Values

	complex 1		complex 2	
method	S_0 *d*(Pt–Pt)/Å	T_1 *d*(Pt–Pt)/Å	S_0 *d*(Pt–Pt)/Å	T_1 *d*(Pt–Pt)/Å
EXAFS	3.34	3.34	3.03	2.60
DFT	3.49	3.50	3.16[a]	2.73[a]
crystal structure	3.268	–	2.908[a]	–

[a]Structure of a geometrically analogous Pt dimer without the NDI group.

The novelty of these results lies in the observation of a net oxidation of the Pt–Pt centers in both **1** and **2**, while simultaneously detecting different Pt–Pt nuclear structural responses to the valence excitation due to the nature of the electronic transitions. The photoinduced Pt–Pt bond formation occurs in only **2** as a result of substantial steric hindrance from pyrazolate –R groups engendering d_{z^2} orbital overlap in the ground state. With ~0.3 Å Pt–Pt distance difference between **1** and **2** in the ground state, the two complexes possess different sets of potential energy surfaces and traverse two different excited-state pathways. When the Pt–Pt distance is about 3.3 Å or greater in the ground state, as in complex **1**, excitation of the LC/MLCT transition does not induce Pt–Pt bond formation due to the lack of $5d_{z^2}$ orbital overlap. In contrast, when the Pt–Pt distance is ~3.0 Å or shorter in the ground state, as in complex **2**, excitation of the MMLCT transition instead drives Pt–Pt bond formation. This is consistent with prior direct measurement of a similar compound with a R = *tert*-butyl (^{t}Bu) group (Figure 1) using XANES structural fitting,[26] which showed a contraction in Pt–Pt distance of 0.23 Å. The differing magnitude of contraction is predicted by DFT calculations[13] and is due to the shorter ground-state Pt–Pt distance in the R = ^{t}Bu complex. These measurements are not capable of directly addressing the distribution of the hole across the two Pt-centers in **1** and **2**, but given the excited-state Pt–Pt contraction in **2** and lack of excited-state Pt–Pt contraction in **1**, the hole is expected to be shared between the two Pt atoms in **2** but localized on a single Pt atom in **1**.

These current results establish a boundary for the ground-state Pt–Pt distance to enable or disable the formation of the Pt–Pt bond in the excited state. Characterizing these effects, both structural and electronic, of metal–metal interactions is essential to understanding the complex excited-state dynamics of systems, both natural and synthetic, that feature multiple transition metal centers. Furthermore, the observation of electron transfer to the NDI acceptor shows the potential of the Pt(II) dimer framework as an electron donor–acceptor system. Future studies will focus on deciphering the effects of different nuclear parameters, such as metal–metal interaction, donor–acceptor orientation, and vibrations, on the electron-transfer process. Identifying key factors that modulate the rate and efficiency of electron transfer will allow for the intelligent design of TMCs for the purpose of solar energy utilization.

CONCLUSION

As a class of materials that shows great promise for use in technologies that hinge upon light–matter interactions, such as OLEDs and photocatalysts, it is necessary to understand the complex structural and electronic dynamics of binuclear TMCs upon photoexcitation. Pt(II) dimers of the form $[Pt(ppy)(\mu\text{-}R_2pz)]_2$ offer a unique structural tunability, and, thus, understanding the interplay between structural components and excited-state dynamics is essential for optimized functionality. By changing the –R group from H to Ph and thus shortening the ground-state Pt–Pt distance, we have modulated the interaction between Pt centers in the dimer, transitioning from a LC/MLCT to MMLCT transition, respectively. Previous work predicted the absence of Pt–Pt contraction upon LC/MLCT excitation[13,15] and presence of Pt–Pt contraction upon MMLCT excitation. Here, using complementary optical and X-ray characterization, especially EXAFS analysis, we showed no Pt–Pt contraction in **1** upon LC/MLCT excitation, but significant Pt–Pt contraction in **2** (3.03 Å to 2.60 Å) upon MMLCT excitation. XANES measurements on both complexes **1** and **2** show oxidation of the Pt centers. This result is essential for understanding the fundamental processes in play that dictate the absorptive and emissive tunability of $[Pt(ppy)(\mu\text{-}R_2pz)]_2$-type dimers. We have also shown the effect of substitution of an electron-acceptor group, NDI, on the ppy ligand to induce charge migration away from the Pt dimer in **2**. This addition leads to a electron transfer away from the Pt dimer and onto NDI, shown by the characteristic NDI radical anion absorption spectrum in the OTA spectra. The CS state rises on the same time scale, or faster, as ISC in the MMLCT states and decays in hundreds of picoseconds, significantly faster than the microsecond decay in Pt dimers without the NDI electron acceptor. This work on charge migration in Pt(II) dimers is foundational for future work aimed at further understanding electron transfer in these types of complexes.

https://doi.org/10.1021/acs.jpca.1c07201
J. Phys. Chem. A XXXX, XXX, XXX–XXX

■ ASSOCIATED CONTENT

Supporting Information

The Supporting Information is available free of charge at https://pubs.acs.org/doi/10.1021/acs.jpca.1c07201.

Supporting Information includes synthetic methods, NMR characterization, supplementary OTA data, time evolution of XANES spectra for the excited states, and detailed descriptions of EXAFS analysis and structural parameters extracted (PDF)

■ AUTHOR INFORMATION

Corresponding Authors

Felix N. Castellano − *Department of Chemistry, North Carolina State University, Raleigh, North Carolina 27695-8204, United States;* orcid.org/0000-0001-7546-8618; Email: fncastel@ncsu.edu

Lin X. Chen − *Department of Chemistry, Northwestern University, Evanston, Illinois 60208, United States; Chemical Science and Engineering Division, Argonne National Laboratory, Lemont, Illinois 60439, United States;* orcid.org/0000-0002-8450-6687; Email: l-chen@northwestern.edu

Authors

Nicholas P. Weingartz − *Department of Chemistry, Northwestern University, Evanston, Illinois 60208, United States; Chemical Science and Engineering Division, Argonne National Laboratory, Lemont, Illinois 60439, United States*

Michael W. Mara − *Department of Chemistry, Northwestern University, Evanston, Illinois 60208, United States; Chemical Science and Engineering Division, Argonne National Laboratory, Lemont, Illinois 60439, United States;* orcid.org/0000-0003-3766-9368

Subhangi Roy − *Department of Chemistry, North Carolina State University, Raleigh, North Carolina 27695-8204, United States*

Jiyun Hong − *Department of Chemistry, Northwestern University, Evanston, Illinois 60208, United States*

Arnab Chakraborty − *Department of Chemistry, North Carolina State University, Raleigh, North Carolina 27695-8204, United States*

Samantha E. Brown-Xu − *Department of Chemistry, Northwestern University, Evanston, Illinois 60208, United States*

Brian T. Phelan − *Chemical Science and Engineering Division, Argonne National Laboratory, Lemont, Illinois 60439, United States;* orcid.org/0000-0002-5849-0319

Complete contact information is available at: https://pubs.acs.org/10.1021/acs.jpca.1c07201

Notes

The authors declare no competing financial interest.

■ ACKNOWLEDGMENTS

The work is funded by the Chemical, Biological, and Geological Sciences Division, Basic Energy Science, Office of Science, the US Department of Energy under contract no. DE-AC02-06CH11357. Use of the Advanced Photon Source, an Office of Science user facility, was supported by the US Department of Energy, Office of Science, Office of Basic Energy Sciences, under contract no. DE-AC02-06CH11357.

■ REFERENCES

(1) Liu, Z.; He, W.; Guo, Z. Metal coordination in photoluminescent sensing. *Chem. Soc. Rev.* **2013**, *42* (4), 1568−1600.

(2) Ortmans, I.; Didier, P.; Kirsch-De Mesmaeker, A. New Charge Transfer Luminescent Polymetallic Complexes of Rhodium(III), Iridium(III), and Ruthenium(II) with the Bridging Ligand 1,4,5,8,9,12-Hexaazatriphenylene. *Inorg. Chem.* **1995**, *34* (14), 3695−3704.

(3) Esswein, A. J.; Nocera, D. G. Hydrogen Production by Molecular Photocatalysis. *Chem. Rev.* **2007**, *107* (10), 4022−4047.

(4) Whittemore, T. J.; Xue, C.; Huang, J.; Gallucci, J. C.; Turro, C. Single-chromophore single-molecule photocatalyst for the production of dihydrogen using low-energy light. *Nat. Chem.* **2020**, *12* (2), 180−185.

(5) Evans, R. C.; Douglas, P.; Winscom, C. J. Coordination complexes exhibiting room-temperature phosphorescence: Evaluation of their suitability as triplet emitters in organic light emitting diodes. *Coord. Chem. Rev.* **2006**, *250* (15), 2093−2126.

(6) Ma, B.; Djurovich, P. I.; Garon, S.; Alleyne, B.; Thompson, M. E. Platinum Binuclear Complexes as Phosphorescent Dopants for Monochromatic and White Organic Light-Emitting Diodes. *Adv. Funct. Mater.* **2006**, *16* (18), 2438−2446.

(7) Ma, B.; Li, J.; Djurovich, P. I.; Yousufuddin, M.; Bau, R.; Thompson, M. E. Synthetic Control of Pt···Pt Separation and Photophysics of Binuclear Platinum Complexes. *J. Am. Chem. Soc.* **2005**, *127* (1), 28−29.

(8) Lin, C.-J.; Liu, Y.-H.; Peng, S.-M.; Shinmyozu, T.; Yang, J.-S. Excimer−Monomer Photoluminescence Mechanochromism and Vapochromism of Pentiptycene-Containing Cyclometalated Platinum(II) Complexes. *Inorg. Chem.* **2017**, *56* (9), 4978−4989.

(9) Liu, K.; Meng, L.; Mo, S.; Zhang, M.; Mao, Y.; Cao, X.; Huang, C.; Yi, T. Colour change and luminescence enhancement in a cholesterol-based terpyridyl platinum metallogel via sonication. *J. Mater. Chem. C* **2013**, *1* (9), 1753−1762.

(10) Prusakova, V.; McCusker, C. E.; Castellano, F. N. Ligand-Localized Triplet-State Photophysics in a Platinum(II) Terpyridyl Perylenediimideacetylide. *Inorg. Chem.* **2012**, *51* (15), 8589−8598.

(11) Mydlak, M.; Mauro, M.; Polo, F.; Felicetti, M.; Leonhardt, J.; Diener, G.; De Cola, L.; Strassert, C. A. Controlling Aggregation in Highly Emissive Pt(II) Complexes Bearing Tridentate Dianionic N∧N∧N Ligands. Synthesis, Photophysics, and Electroluminescence. *Chem. Mater.* **2011**, *23* (16), 3659−3667.

(12) Yam, V. W.; Chan, K. H.; Wong, K. M.; Zhu, N. Luminescent platinum(II) terpyridyl complexes: effect of counter ions on solvent-induced aggregation and color changes. *Chem. - Eur. J.* **2005**, *11* (15), 4535−43.

(13) Brown-Xu, S. E.; Kelley, M. S. J.; Fransted, K. A.; Chakraborty, A.; Schatz, G. C.; Castellano, F. N.; Chen, L. X. Tunable Excited-State Properties and Dynamics as a Function of Pt−Pt Distance in Pyrazolate-Bridged Pt(II) Dimers. *J. Phys. Chem. A* **2016**, *120* (4), 543−550.

(14) Chakraborty, A.; Deaton, J. C.; Haefele, A.; Castellano, F. N. Charge-Transfer and Ligand-Localized Photophysics in Luminescent Cyclometalated Pyrazolate-Bridged Dinuclear Platinum(II) Complexes. *Organometallics* **2013**, *32* (14), 3819−3829.

(15) Rachford, A. A.; Castellano, F. N. Thermochromic Absorption and Photoluminescence in [Pt(ppy)(μ-Ph2pz)]2. *Inorg. Chem.* **2009**, *48* (23), 10865−10867.

(16) Gray, H. B.; Zalis, S.; Vlcek, A. Electronic structures and photophysics of d.sup.8-d.sup.8 complexes. *Coord. Chem. Rev.* **2017**, *345*, 297.

(17) van der Veen, R. M.; Cannizzo, A.; van Mourik, F.; Vlček, A.; Chergui, M. Vibrational Relaxation and Intersystem Crossing of Binuclear Metal Complexes in Solution. *J. Am. Chem. Soc.* **2011**, *133* (2), 305−315.

(18) Roundhill, D. M.; Gray, H. B.; Che, C. M. Pyrophosphito-bridged diplatinum chemistry. *Acc. Chem. Res.* **1989**, *22* (2), 55−61.

(19) Chergui, M. On the interplay between charge, spin and structural dynamics in transition metal complexes. *Dalton Transactions.* **2012**, *41* (42), 13022−13029.
(20) Saito, K.; Nakao, Y.; Sakaki, S. Theoretical Study of Pyrazolate-Bridged Dinuclear Platinum(II) Complexes: Interesting Potential Energy Curve of the Lowest Energy Triplet Excited State and Phosphorescence Spectra. *Inorg. Chem.* **2008**, *47* (10), 4329−4337.
(21) Sazanovich, I. V.; Best, J.; Scattergood, P. A.; Towrie, M.; Tikhomirov, S. A.; Bouganov, O. V.; Meijer, A. J. H. M.; Weinstein, J. A. Ultrafast photoinduced charge transport in Pt(ii) donor−acceptor assembly bearing naphthalimide electron acceptor and phenothiazine electron donor. *Phys. Chem. Chem. Phys.* **2014**, *16* (47), 25775−25788.
(22) Han, M.; Tian, Y.; Yuan, Z.; Zhu, L.; Ma, B. A phosphorescent molecular "butterfly" that undergoes a photoinduced structural change allowing temperature sensing and white emission. *Angew. Chem., Int. Ed.* **2014**, *53* (41), 10908−12.
(23) Lingerfelt, D. B.; Lestrange, P. J.; Radler, J. J.; Brown-Xu, S. E.; Kim, P.; Castellano, F. N.; Chen, L. X.; Li, X. Can Excited State Electronic Coherence Be Tuned via Molecular Structural Modification? A First-Principles Quantum Electronic Dynamics Study of Pyrazolate-Bridged Pt(II) Dimers. *J. Phys. Chem. A* **2017**, *121* (9), 1932−1939.
(24) Radler, J. J.; Lingerfelt, D. B.; Castellano, F. N.; Chen, L. X.; Li, X. Role of Vibrational Dynamics on Excited-State Electronic Coherence in a Binuclear Platinum Complex. *J. Phys. Chem. A* **2018**, *122* (23), 5071−5077.
(25) Valentine, A. J. S.; Radler, J. J.; Mills, A.; Kim, P.; Castellano, F. N.; Chen, L. X.; Li, X. Resolving the ultrafast intersystem crossing in a bimetallic platinum complex. *J. Chem. Phys.* **2019**, *151* (11), 114303.
(26) Lockard, J. V.; Rachford, A. A.; Smolentsev, G.; Stickrath, A. B.; Wang, X.; Zhang, X.; Atenkoffer, K.; Jennings, G.; Soldatov, A.; Rheingold, A. L.; et al. Triplet Excited State Distortions in a Pyrazolate Bridged Platinum Dimer Measured by X-ray Transient Absorption Spectroscopy. *J. Phys. Chem. A* **2010**, *114* (48), 12780−12787.
(27) Haldrup, K.; Dohn, A. O.; Shelby, M. L.; Mara, M. W.; Stickrath, A. B.; Harpham, M. R.; Huang, J.; Zhang, X.; Møller, K. B.; Chakraborty, A.; et al. Butterfly Deformation Modes in a Photoexcited Pyrazolate-Bridged Pt Complex Measured by Time-Resolved X-Ray Scattering in Solution. *J. Phys. Chem. A* **2016**, *120* (38), 7475−7483.
(28) Kim, P.; Kelley, M. S.; Chakraborty, A.; Wong, N. L.; Van Duyne, R. P.; Schatz, G. C.; Castellano, F. N.; Chen, L. X. Coherent Vibrational Wavepacket Dynamics in Platinum(II) Dimers and Their Implications. *J. Phys. Chem. C* **2018**, *122* (25), 14195−14204.
(29) Mewes, L.; Ingle, R. A.; Megow, S.; Böhnke, H.; Baranoff, E.; Temps, F.; Chergui, M. Ultrafast Intersystem Crossing and Structural Dynamics of [Pt(ppy)(μ-tBu2pz)]2. *Inorg. Chem.* **2020**, *59* (20), 14643−14653.
(30) Cho, S.; Mara, M. W.; Wang, X.; Lockard, J. V.; Rachford, A. A.; Castellano, F. N.; Chen, L. X. Coherence in Metal-Metal-to-Ligand-Charge-Transfer Excited States of a Dimetallic Complex Investigated by Ultrafast Transient Absorption Anisotropy. *J. Phys. Chem. A* **2011**, *115* (16), 3990−3996.
(31) Kim, P.; Valentine, A. J. S.; Roy, S.; Mills, A. W.; Chakraborty, A.; Castellano, F. N.; Li, X.; Chen, L. X. Ultrafast Excited-State Dynamics of Photoluminescent Pt(II) Dimers Probed by a Coherent Vibrational Wavepacket. *J. Phys. Chem. Lett.* **2021**, *12* (29), 6794−6803.
(32) Fransted, K. A.; Jackson, N. E.; Zong, R.; Mara, M. W.; Huang, J.; Harpham, M. R.; Shelby, M. L.; Thummel, R. P.; Chen, L. X. Ultrafast Structural Dynamics of Cu(I)-Bicinchoninic Acid and Their Implications for Solar Energy Applications. *J. Phys. Chem. A* **2014**, *118* (45), 10497−10506.
(33) Hong, J.; Fauvell, T. J.; Helweh, W.; Zhang, X.; Chen, L. X. Investigation of the photoinduced axial ligation process in the excited state of nickel(II) phthalocyanine. *J. Photochem. Photobiol., A* **2019**, *372*, 270−278.
(34) Chen, L. X.; Zhang, X.; Shelby, M. L. Recent advances on ultrafast X-ray spectroscopy in the chemical sciences. *Chemical Science.* **2014**, *5* (11), 4136−4152.
(35) Ravel, B.; Newville, M. ATHENA, ARTEMIS, HEPHAESTUS: data analysis for X-ray absorption spectroscopy using IFEFFIT. *J. Synchrotron Radiat.* **2005**, *12*, 537−541.
(36) Newville, M. IFEFFIT: interactive XAFS analysis and FEFF fitting. *J. Synchrotron Radiat.* **2001**, *8* (2), 322−324.
(37) Tenderholt, A.; Hedman, B.; Hodgson, K. O. PySpline: A Modern, Cross□Platform Program for the Processing of Raw Averaged XAS Edge and EXAFS Data. *AIP Conference Proceedings.* **2006**, *882* (1), 105−107.
(38) Bhosale, S. V.; Jani, C. H.; Langford, S. J. Chemistry of naphthalene diimides. *Chem. Soc. Rev.* **2008**, *37* (2), 331−342.
(39) Gosztola, D.; Niemczyk, M. P.; Svec, W.; Lukas, A. S.; Wasielewski, M. R. Excited Doublet States of Electrochemically Generated Aromatic Imide and Diimide Radical Anions. *J. Phys. Chem. A* **2000**, *104* (28), 6545−6551.
(40) Vagnini, M. T.; Mara, M. W.; Harpham, M. R.; Huang, J.; Shelby, M. L.; Chen, L. X.; Wasielewski, M. R. Interrogating the photogenerated Ir(iv) state of a water oxidation catalyst using ultrafast optical and X-ray absorption spectroscopy. *Chemical Science.* **2013**, *4* (10), 3863−3873.
(41) Vagnini, M. T.; Smeigh, A. L.; Blakemore, J. D.; Eaton, S. W.; Schley, N. D.; D'Souza, F.; Crabtree, R. H.; Brudvig, G. W.; Co, D. T.; Wasielewski, M. R. Ultrafast photodriven intramolecular electron transfer from an iridium-based water-oxidation catalyst to perylene diimide derivatives. *Proc. Natl. Acad. Sci. U. S. A.* **2012**, *109* (39), 15651.
(42) Castellano, F. N. Transition metal complexes meet the rylenes. *Dalton Transactions.* **2012**, *41* (28), 8493−8501.

https://doi.org/10.1021/acs.jpca.1c07201
J. Phys. Chem. A XXXX, XXX, XXX−XXX